Optics Letters

Tamm-plasmon polaritons in one-dimensional photonic quasi-crystals

Mukesh Kumar Shukla* and Ritwick Das

School of Physical Sciences, National Institute of Science Education and Research, HBNI, Jatni 752050, India
**Corresponding author: mukesh.s@niser.ac.in*

Received 7 November 2017; revised 4 December 2017; accepted 17 December 2017; posted 19 December 2017 (Doc. ID 312979); published 16 January 2018

We present an investigation to ascertain the existence of Tamm-plasmon-polariton-like modes in one-dimensional (1D) quasi-periodic photonic systems. Photonic bandgap formation in quasi-crystals is essentially a consequence of long-range periodicity exhibited by multilayers and, thus, it can be explained using the dispersion relation in the Brillouin zone. Defining a "Zak"-like topological phase in 1D quasi-crystals, we propose a recipe to ascertain the existence of Tamm-like photonic surface modes in a metal-terminated quasi-crystal lattice. Additionally, we also explore the conditions of efficient excitation of such surface modes along with their dispersion characteristics.

OCIS codes: (240.0240) Optics at surfaces; (240.5420) Polaritons; (240.6690) Surface waves; (230.1480) Bragg reflectors.

https://doi.org/10.1364/OL.43.000362

Complex dielectric configurations have attracted considerable attention due to their applications and resemblance to naturally existing systems. For example, a conventional periodically stratified medium, widely known as one-dimensional photonic crystal (1D-PC) or, alternately, distributed-Bragg reflector (DBR), exhibits photonic bandgap (PBG) in well-defined propagation directions as a consequence of Bragg scattering [1]. Such PC-based configurations support interesting optical surface states (OSS) in transverse electric (TE) as well as transverse magnetic (TM) polarizations [2]. Using the topological properties of 1D-PC, which is essentially characterized by "Zak"-phase, the existence of OSS has been predicted and classified in terms of symmetry exhibited by 1D periodicity [3,4]. Interestingly, the configurations with apparently broken translational symmetry in dielectric arrangement, but that follow a mathematically defined sequence such as Fibonacci or period-doubling lattices, exhibit PBG and transmission bands that closely resemble a periodic system. This leads to interesting dispersion and absorption characteristics that apparently improve their functionality in various applications [5–10]. A few recent investigations have shown that photonic quasi-crystals provide better performance in an optical sensing configuration as compared to DBR-based configurations by optimally engineering the dielectric layer sequence [11]. Also, a Fibonacci-sequence (FS)-based quasi-crystal geometry has been found to add additional degrees of freedom in designing devices for nano-photonics, biochemical sensing, nonlinear optical processes, and slow light generation [12–15].

From a different perspective, the field of plasmonics has experienced an enormous growth, and it forms a crucial ingredient for various applications, such as sensor designing, near-field microscopy, nonlinear optics, etc. [16,17]. Metallo-dielectric geometries supporting surface plasmon polariton (SPP) modes form the backbone of such applications [18]. SPP modes require dispersion-compensating elements such as prisms and gratings for efficient excitation as well as manipulation. The polarization dependence of SPP modes puts additional constraint on devising complex configurations. The bottlenecks imposed by SPP modes could be circumvented by Tamm-plasmon-polariton (TPP)-based architectures [19,20]. TPP modes are strongly confined OSS that exist at the interface of material exhibiting negative dielectric constant (e.g., metal) and DBR. The TPP modes could be excited using free-space plane waves for both the orthogonal polarizations [21]. Also, due to unique dispersion properties exhibited by TPP modes, they have been utilized in a variety of applications, such as optical switching, optical sensing, and harmonic generation, as well as controlling spontaneous emission [21–27]. Until now, to the best of our knowledge, TPP modes have been investigated and excited at the interface of 1D-PC-based geometries and plasmon-active metals such as Au, Ag, and Al [19,20,25]. In the present work, we explore the possibility of the existence of TPP-like modes at the interface of 1D quasi-crystals such as FS lattice and plasmon-active metal with an emphasis to topological properties of bulk photonic quasi-crystal.

We have considered two dielectric materials, SiO_2 (denoted as "A") and Ta_2O_5 (denoted as "B"), having thicknesses "d_A" (refractive index: n_A) and "d_B" (refractive index: n_B), respectively, arranged in a stacked multilayer configuration (see Fig. 1). Layers A and B are distributed along the x axis (beam-propagation direction). For the present study, we consider a plane *em*-wave to be normally incident on the geometry, and, for simplicity, the thicknesses (d_A and d_B) are assumed to satisfy the condition $k_A d_A = k_B d_B = \frac{\pi}{2}$, where $k_A = \frac{\omega}{c} n_A$

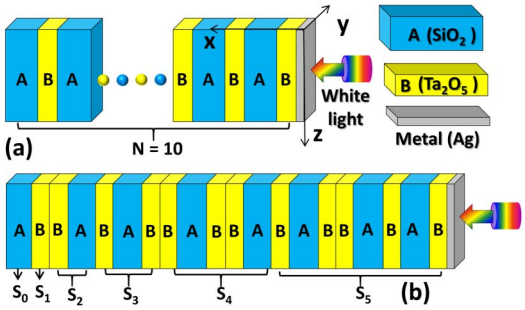

Fig. 1. Schematic of sequences in horizontally stacked multilayer configuration. (a) Silver (Ag) capped conventional distributed-Bragg reflector (DBR) with $N = 10$ unit cells; and (b) Fibonacci-sequence-based distributed reflector with terminating Ag layer (Ag-FS-DR) with a sequence defined as $S_0S_1S_2S_3S_4S_5$).

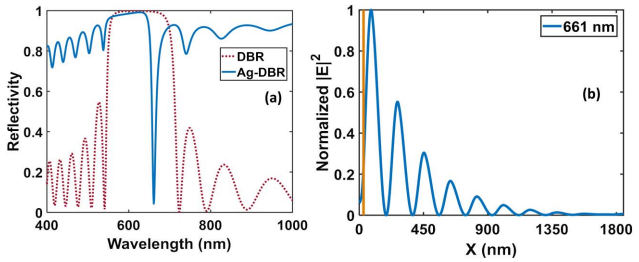

Fig. 2. (a) Reflection spectra of DBR and Ag-DBR and (b) corresponding mode-field intensity distribution at $\lambda_r = 661$ nm. Vertical line (brown color) in (b) indicates the metal–dielectric interface.

and $k_B = \frac{\omega}{c} n_B$ are the wavevectors in A and B layers, respectively. The reflection (or transmission) spectrum for the multilayer configuration is obtained by using transfer matrix formulation where a 2×2 matrix (T_j) connects the electric field in two adjacent layers. The matrix T_j is defined as follows [28]:

$$T_j = \begin{bmatrix} \cos\delta_j & -r_j^{-1}\sin\delta_j \\ r_j \sin\delta_j & \cos\delta_j \end{bmatrix}, \quad \textbf{(1)}$$

where $r_j = 1$ if the jth layer is of type A, or $r_j = n_A/n_B$ if it is of type B. Here, $\delta_j = \frac{2\pi}{\lambda} n_j d_j$ $(j = A, B)$ is the accumulated phase shift due to *em*-wave propagation through each layer. Light propagation through N layers of a multilayer geometry would, therefore, be represented by $T_N(\delta)$, which is essentially a product of an appropriate sequence of T_j matrices [Eq. (1)]. For a multilayer configuration that is sandwiched between two semi-infinite media ("air" in our case), the transmitted intensity $T(\delta)$ is given by

$$T(\delta) = [(m_{11} + m_{22})^2 + (m_{21} - m_{12})^2]/4, \quad \textbf{(2)}$$

where m_{pq} (p or $q = 1, 2$) are the elements of $T_N(\delta)$. The metal layer (Ag in this case) is assumed to form the last (terminating) layer as shown in Fig. 1 and abbreviated as "M." To begin with, we define a conventional DBR with sequence *ABABABABABABABABABAB* in Fig. 1(a) for elucidating significant aspects in the reflection (transmission) spectrum, which will be employed further when we discuss the quasi-crystal in the next section. In order to obtain the reflection spectrum of DBR, the refractive indices of SiO_2 and Ta_2O_5 have been adopted from [29,30], respectively, whereas the dispersion of Ag has been obtained from [31]. We employ the aforementioned formulation with material dispersion for obtaining the reflection $(1 - T(\delta))$ spectrum of a conventional DBR [Fig. 1(a)] and metal (Ag)-coated DBR [Fig. 1(a)], which is shown in Fig. 2(a). Here, $N = 10$ is the number of unit cells, and all the calculations have been performed assuming DBR central wavelength to be 600 nm, which results in $d_A = 125$ nm and $d_B = 60$ nm. It could be easily ascertained that the reflection spectrum for Ag-DBR geometry is characterized by a sharp reflection minimum at $\lambda_r = 661$ nm within the PBG depicting the excitation of a TPP mode at the Ag–DBR interface [2,19]. The electric field distribution at TPP resonance wavelength, $\lambda_r = 661$ nm, is shown in Fig. 2(b), where it could be observed that the field has a decaying envelope in the DBR as well as Ag layer. It is worthwhile to note that the existence of TPP mode at the Ag-DBR interface is essentially governed by the surface impedance (Z_{DBR}) of DBR for frequencies within PBG. In other words, the necessary condition for realizing an OSS is $Z_{\mathrm{DBR}} + Z_m = 0$, where Z_m is the surface impedance for metal (Ag). This manifests into $\phi_{\mathrm{DBR}} + \phi_m = 0$ for the existence of an OSS, where ϕ_{DBR} and ϕ_m are the reflection phases for DBR and metal, respectively. In general, $Z_{\mathrm{DBR}} = \frac{1+r_{\mathrm{DBR}}}{1-r_{\mathrm{DBR}}} Z_0$, where $r_{\mathrm{DBR}} = \frac{Q}{P+\tau}$ is the reflection coefficient for DBR, and Z_0 is vacuum impedance. Here, $\tau = \frac{\sinh[(N-1)K_i\Lambda]}{\sinh[(N)K_i\Lambda]}$, $P = e^{ik_Ad_A}[\cos(k_Bd_B) + \frac{i}{2}(\frac{k_B}{k_A} + \frac{k_A}{k_B})\sin(k_Bd_B)]$ and $Q = e^{-ik_Ad_A}[\frac{i}{2}(\frac{k_A}{k_B} - \frac{k_B}{k_A})\sin(k_Bd_B)]$, K_i is the imaginary part of Bloch wavenumber (K), and $k_{A,B}$ are components of wavevector along x direction [4,32]. Within the PBG of DBR with a very large number of unit cells, $Z_{\mathrm{DBR}} = i\zeta$ is a purely imaginary number, and, therefore, the reflection phase (ϕ_{DBR}) within the PBG would be given by $\phi_{\mathrm{DBR}} = \frac{\pi}{2} - 2\tan^{-1}(\zeta)$ [4]. It is interesting to note that the ϕ_{DBR} and ζ share the same sign, which, in turn, is dictated by the topological properties of the transmission bands in 1D-PC. Alternately, the sign of ϕ_{DBR} (and ζ) within the first PBG is given by $\mathrm{Sgn}[\phi_{\mathrm{DBR}}] = -\exp(i\theta_0^{\mathrm{zak}})$, where θ_0^{zak} is the "Zak" phase (or topological phase) of the first transmission band. Since, ϕ_m, in general, is negative at optical frequencies, the "Zak" phase of $\theta_0^{\mathrm{zak}} = \pi$ for the lowest transmission $(m = 1)$ band is necessary to excite a TPP mode. With reference to Fig. 2(a), the "Zak" phase for the lowest transmission band $(m = 1)$ is given as $\exp(i\theta_0^{\mathrm{zak}}) = \mathrm{Sgn}[1 - \frac{n_B^2}{n_A^2}]$, which results in $\theta_0^{\mathrm{zak}} = \pi$, and, consequently, we obtain a TPP mode at the Ag–DBR interface.

In order to define the quasi-crystalline sequence, we adopt the recipe prescribed by Albuquerque and Cottam [33], which comprises all finite words S_n for describing the sequence. For example, we consider a FS that is defined by a word count rule, $S_n = S_{n-1}S_{n-2}$ for $n \geq 2$ with $S_0 = A$ and $S_1 = B$. Consequently, the first few strings of FS are S_0:A; S_1:B; S_2:BA; S_3:BAB; S_4:$BABBA$; and S_5:$BABBABAB$. In this example, we consider a multilayer stack with $S_0S_1S_2S_3S_4S_5$ [as shown in Fig. 1(b)] with a top metal (Ag) layer of 30 nm, which is denoted by M. The complete distributed-reflector (DR) sequence defining the multilayer configuration could be written as "*ABBABABBABBABABBABABM*," which will henceforth be abbreviated as Ag-FS-DR. The number of layers in Ag-FS-DR is 21, which is identical to that contained in

the Ag-DBR configuration [see Fig. 1(a)]. Further, A and B layer thicknesses in FS-DR were chosen identical to that for DBR so as to draw straightforward comparison between their reflection spectra, i.e., $d_A = 125$ nm and $d_B = 60$ nm. It is worthwhile to point out that higher-order strings in FS would result in sharper band edges owing to a higher number of constituent layers [15]. In Fig. 3(a), the reflection spectrum of FS-DR geometry is plotted where it is apparent that there exists a PBG extending from ∼600 to 900 nm with smoother band edges in comparison with conventional DBR [Fig. 2(a)] for identical geometrical parameters. The formation of PBG in FS-DR lattice is essentially a consequence of long-range periodicity exhibited by quasi-periodic configurations. For example, the FS discussed here could be represented as $XYXY|YXYX$, where $X = AB$ and $Y = BAB$. This sequence is characterized by a periodic unit "XY" and an inherent center for inversion symmetry about the vertical line. Such a long-range periodicity essentially manifests into an extended PBG [shown in Fig. 3(a)], and the inversion symmetry plane gives rise to a "dimer-like" chain at the center of FS-DR lattice. Consequently, we obtain a sharp resonance at $\lambda_s = 665$ nm (within the PBG) depicting a cavity-mode being supported inherently by FS-DR photonic lattice [34]. The E-field intensity variation for the mode $\lambda_s = 665$ nm in Fig. 3(b) confirms a cavity-mode-like variation with the field maxima located at central Y-layer. On the other hand, E-field intensity distribution at $\lambda = 593$ nm distinctly depicts a band-edge mode confirming a broadband PBG extending from ∼600 to 900 nm. In order to obtain a physical insight into the topological properties of FS-D geometry, we attempted to obtain the topological phase ("Zak" phase) of the lowest-order ($m = 1$) transmission band. However, it is worth noting that the refractive indices "n_X" and "n_Y" (refractive indices of X and Y layers, respectively) are not uniquely defined in the quasi-periodic sequence, and, consequently, the "Zak"-like phase for $m = 1$ band cannot be directly obtained. A plausible alternate would be to obtain the reflection spectrum of Ag–FS–DR geometry. This is shown in Fig. 3(c) where sharp reflectivity minima within the PBG are observed, which is a signature of

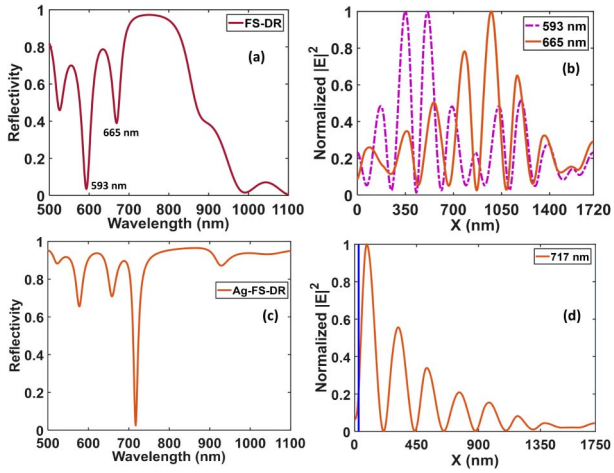

Fig. 3. (a) Reflection spectra of FS-DR; (b) E-field intensity distribution at $\lambda_r = 593$ nm and $\lambda_r = 665$ nm characterizing a band-edge mode and cavity-mode, respectively; (c) reflection spectrum of Ag-FS-DR geometry; and (d) E-field intensity distribution at $\lambda_r = 717$ nm. Vertical line (blue color) in (d) represents the metal–dielectric interface.

OSS. The E-field intensity distribution at $\lambda_r = 717$ nm in Fig. 3(d) clearly depicts field maxima at the Ag–B (layer) interface with a decaying envelope in the quasi-periodic undulation of FS lattice. Also, it is worthwhile to note that the linewidth ($\Delta\lambda$) of TPP-like resonance in Ag–FS–DR is $\Delta\lambda \approx 14$ nm, whereas it was $\Delta\lambda \approx 10$ nm for the Ag–DBR configuration (Fig. 1). Accordingly, the quality factor, which is defined as $Q_F = \frac{\lambda_r}{\Delta\lambda}$, is estimated to be $Q_F \approx 50$ and $Q_F \approx 60$ for Ag–FS–DR and Ag–DBR, respectively. Hence, finesse of FS–DR is slightly smaller than that for DBR when the total number of layers is the same in both configurations. This is primarily due to a fewer number of XY units in 1D quasi-crystal geometry.

The presence of TPP-like mode in the Ag–FS–DR geometry could be employed for ascertaining the topological properties of 1D quasi-crystals using the recipe described in the case of 1D-PC. In other words, we attributed the presence of TPP-mode in the Ag–DBR configuration due to $\theta_0^{\text{zak}} = \pi$ for the lowest ($m = 1$) transmission band of 1D-PC. On a similar note, the observation of TPP-like mode (or an OSS) in the first PBG of Ag–FS–DR geometry could be attributed to $\theta_0^{\text{zak}} = \pi$ for the lowest $m = 1$ transmission band. Subsequently, we would like to assert that the presence of TPP-like modes in higher-order PBG of photonic quasi-crystals could be employed for ascertaining "Zak" phase and hence the topological properties of lower-order transmission bands. It could also be noted that the surface impedances ($Z_{\text{FS-DR}}$ as well as Z_m) alter significantly when the geometrical parameters of FS–DR or the metal layer change. This was apparent in the case of 1D-PC or DBR where Z_{DBR} is a function of thicknesses d_A, d_B, as well as N.

As discussed in the previous section, it is important to appreciate that coupling efficiency to TPP modes critically depends on the geometrical parameters of the DR architecture, as well as the metal [35,36]. This could be derived from the dependence of reflection (or transmission) phases of *em*-waves in periodic as well as quasi-periodic photonic lattice. In order to appreciate that, we have plotted a map representing reflectivity for various metal thicknesses in the case of Ag–DBR and Ag–FS–DR geometry with $d_A = 120$ nm and $d_B = 60$ nm in Figs. 4(a) and 4(b), respectively. It is apparent from Fig. 4(a) that the most efficient excitation (R_{min}) of TPP mode takes place for metal thickness in the range 30–40 nm for the Ag–DBR case, which is pushed down to 20–30 nm in the case of Ag–FS–DR. Also, it is worthwhile to note that the TPP resonance exhibits a blue shift as a function of metal layer thickness. Additionally, the TPP resonance widths ($\Delta\lambda$) in both figures tend to reduce with increase in Ag layer thickness. Both observations are primarily a consequence of increase in reflectivity of the Ag layer (for higher d_{Ag}), which enhances mode-field confinement at the Ag–DR. In order to gain some physical insight for Figs. 4(a) and 4(b), it is worthwhile to recall that $\phi_m + \phi_{\text{FS-DR}} = 0$ (or $Z_m + Z_{\text{FS-DR}} = 0$) for the first PBG in order to realize TPP-like resonance. Here, $\phi_m = \text{Arg}(r_m)$, where $r_m = \frac{r_1 + r_2 \exp(2ik_0 n_{\text{Ag}} d_{\text{Ag}})}{1 + r_1 r_2 \exp(2ik_0 n_{\text{Ag}} d_{\text{Ag}})}$, where r_1 and r_2 are complex reflection coefficients at two interfaces of a thin metal layer of thickness d_{Ag}, and k_0 is the free-space wavenumber. Consequently, ϕ_m varies as a function of d_{Ag}, which would affect the resonance condition. In fact, $R_{\text{min}} \approx 0$ represents a condition when $\phi_M + \phi_{\text{DR}}$ is closest to 0 for the optimum value of d_{Ag}. On the other hand, R_{min} tends to increase for the non-optimum value of d_{Ag} in Fig. 4, which is essentially

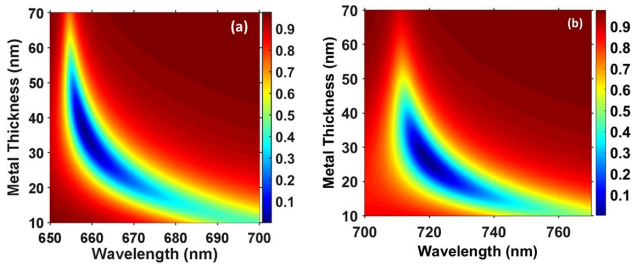

Fig. 4. Variation of reflectivity as a function of wavelength and Ag-layer (metal) thickness for (a) Ag-DBR and (b) Ag-FS-DR.

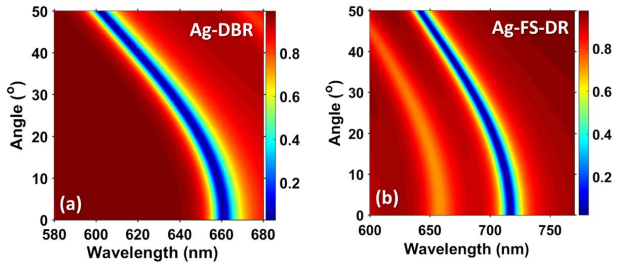

Fig. 5. Variation of reflectivity of TE-polarized *em*-field as a function of wavelength and angle of incidence (AOI) for (a) Ag-DBR and (b) Ag-FS-DR when $d_{\mathrm{Ag}} = 30$ nm.

due to significant deviation of reflection phases from condition $\phi_M + \phi_{\mathrm{DR}} = 0$ when d_{Ag} varies.

In order to appreciate the dispersive properties of TPP-like modes in quasi-periodic configurations, we plot a map of reflection spectra for TE-polarized *em*-waves with angles of incidence (AOI) for Ag–DBR and Ag–FS–DR in Figs. 5(a) and 5(b), respectively. The TPP-like resonance undergoes a blue shift at higher AOI which is essentially due to a non-zero planar component of wavevector. It is important to note that the angular dispersion of TPP-like modes in Ag–FS–DR, is discernibly weaker as compared to that for TPP mode in Ag–DBR geometry. Such a behavior is primarily attributed to nominal change in field distribution for modes in quasi-periodic lattice as a function of frequency [37]. The weak dispersion characteristics in quasi-periodic configurations could be useful devising miniaturized dispersion compensating elements with enhanced functionality.

In conclusion, we have investigated the existence TPP-like modes in photonic quasi-periodic configurations. Since optical surface modes are dictated by topological properties of quasi-periodic geometry, we ascertain the "Zak" phase of the lowest ($m = 1$) transmission band of FS-based DR from the presence of TPP-like mode in the first PBG. The TPP-like mode in the Ag–FS–DR configuration exhibits weaker dispersion characteristics in comparison to conventional TPP modes in Ag–DBR geometries.

REFERENCES

1. P. Yeh, *Optical Waves in Layered Media* (Wiely-VCH, 2005).
2. A. P. Vinogradov, A. V. Dorofeenko, S. G. Erokhin, M. Inoue, A. A. Lisyansky, A. M. Merzlikin, and A. B. Granovsky, Phys. Rev. B **74**, 045128 (2006).
3. J. Zak, Phys. Rev. Lett. **62**, 2747 (1989).
4. M. Xiao, Z. Zhang, and C. T. Chan, Phys. Rev. X **4**, 021017 (2014).
5. J. Dong, M. Chang, X. Huang, Z. H. Hang, Z. Zhong, W. Chen, Z. Huang, and C. T. Chan, Phys. Rev. Lett. **114**, 163901 (2015).
6. C. Janot, *Quasicrystals: A Premier*, 2nd ed. (Clarendon, 1994).
7. W. S. Gao, M. Xiao, C. T. Chan, and W. Y. Tam, Opt. Lett. **40**, 5259 (2015).
8. K. H. Choi, C. W. Ling, K. F. Lee, Y. H. Tsang, and K. H. Fung, Opt. Lett. **41**, 1644 (2016).
9. A. M. Vyunishev, P. S. Pankin, S. E. Svyakhovskiy, I. V. Timofeev, and S. Y. Vetrov, Opt. Lett. **42**, 3602 (2017).
10. Q. Wang, M. Xiao, H. Liu, S. Zhu, and C. T. Chan, Phys. Rev. B **93**, 041415(R) (2016).
11. L. Moretti, I. Rea, L. De Stefano, and I. Rendina, Appl. Phys. Lett. **90**, 191112 (2007).
12. X. Hui and C. Yu, Photon. Res. **5**, 11 (2017).
13. W. Cai, A. P. Vasudev, and M. L. Brongersma, Science **333**, 1720 (2011).
14. B. Spackova, P. Wrobel, M. Bockova, and J. Homola, Proc. IEEE **104**, 2380 (2016).
15. L. D. Negro, C. J. Oton, Z. Gaburro, L. Pavesi, P. Johnson, A. Lagendijk, R. Righini, M. Colocci, and D. S. Wiersma, Phys. Rev. Lett. **90**, 055501 (2003).
16. S. A. Maier, *Plasmonics: Fundamentals and Applications* (Springer, 2007).
17. M. I. Stockman, Opt. Express **19**, 22029 (2011).
18. W. L. Barnes, A. Dereux, and T. W. Ebbesen, Nature **424**, 824 (2003).
19. M. Kaliteevski, I. Iorsh, S. Brand, R. A. Abram, I. A. Shelykh, and A. V. Kavokin, Phys. Rev. B **76**, 165415 (2007).
20. M. E. Sasin, R. P. Seisyan, M. A. Kalitteevski, S. Brand, R. A. Abram, J. M. Chamberlain, A. Y. Egorov, A. P. Vasil'ev, V. S. Mikhrin, and A. V. Kavokin, Appl. Phys. Lett. **92**, 251112 (2008).
21. Y. Chen, D. Zhang, L. Zhu, R. Wang, P. Wang, H. Ming, R. Badugu, and J. R. Lakowicz, Optica **1**, 407 (2014).
22. O. Gazzano, S. Michaelis de Vasconcellos, K. Gauthron, C. Symonds, P. Voisin, J. Bellessa, A. Lemaître, and P. Senellart, Appl. Phys. Lett. **100**, 232111 (2012).
23. B. I. Afinogenov, V. O. Bessonov, and A. A. Fedyanin, Opt. Lett. **39**, 6895 (2014).
24. C. H. Xue, H. T. Jiang, H. Lu, G. Q. Du, and H. Chen, Opt. Lett. **38**, 959 (2013).
25. C. Symonds, A. Lemaître, P. Senellart, M. H. Jomaa, S. Aberra Guebrou, E. Homeyer, G. Brucoli, and J. Bellessa, Appl. Phys. Lett. **100**, 121122 (2012).
26. S. Kumar, M. K. Shukla, P. S. Maji, and R. Das, J. Phys. D **50**, 375106 (2017).
27. E. Yablonovitch, Phys. Rev. Lett. **58**, 2059 (1987).
28. L. Kroon, E. Lennholm, and R. Riklund, Phys. Rev. B **66**, 094204 (2002).
29. G. Ghosh, M. Endo, and T. Iwasaki, J. Lightwave Technol. **12**, 1338 (1994).
30. T. J. Bright, J. I. Watjen, Z. M. Zhang, C. Muratore, A. A. Voevodin, D. I. Koukis, D. B. Tanner, and D. J. Arenas, J. Appl. Phys. **114**, 083515 (2013).
31. P. B. Johnson and R. W. Christy, Phys. Rev. B **6**, 4370 (1972).
32. P. Yeh, A. Yariv, and C. S. Hong, J. Opt. Soc. Am. **67**, 423 (1977).
33. E. L. Albuquerque and M. G. Cottam, Phys. Rep. **376**, 225 (2003).
34. R. W. Peng, Y. M. Liu, X. Q. Huang, F. Qiu, M. Wang, A. Hu, S. S. Jiang, D. Feng, L. Z. Ouyang, and J. Zou, Phys. Rev. B **69**, 165109 (2004).
35. B. Auguie, A. Bruchhausen, and A. Fainstein, J. Opt. **17**, 035003 (2015).
36. R. Das, T. Srivastava, and R. Jha, Opt. Lett. **39**, 896 (2014).
37. T. Hattori, N. Tsurumachi, S. Kawato, and H. Nakatsuka, Phys. Rev. B **50**, 4220 (1994).